Colloids and Surfaces A: Physicochemical and Engineering Aspects, 81 (1993) 65–81
0927-7757/93/$06.00

Concentrated dispersions of charged colloidal particles: sedimentation, ultrafiltration and diffusion[α]

D.N. Petsev[a], V.M. Starov[b], I.B. Ivanov[a,*]

[a] *Laboratory of Thermodynamics and Physico-chemical Hydrodynamics, Faculty of Chemistry, University of Sofia, 1126 Sofia, Bulgaria*
[b] *Department of Mathematics, Moscow Institute for Food Technology, Moscow, Russian Federation*

(Received 5 October 1992; accepted 6 June 1993)

Abstract

The formation and structure of sedimentation and/or filtration layers built up by charged colloidal particles were studied. For that purpose a theoretical model based on the force balance on a given particle in the layer was developed. The colloid stability problem and appearance of coagulation were considered. The hydrodynamic permeability of a filtration layer, consisting of charged particles, was calculated for different values of the electrolyte concentration, filtration rate, particle surface potential and radius. A simple expression for estimation of the collective diffusion coefficient of charged colloidal particles at relatively high volume fractions was also proposed.

Key words: Charged colloidal particles; Concentrated dispersions; Diffusion; Sedimentation; Ultrafiltration

1. Introduction

Colloidal dispersions have been of increasing interest during recent years. One reason for this fact is their relation to different industrial activities: ceramics fabrication, production of paints and coating dispersions, biotechnology and many others. Besides, different challenging fundamental problems, concerning colloidal suspensions, exist. The difficulties in the theoretical studies of colloidal dispersions arise mainly from the complex hydrodynamics and the almost inevitable presence of long-range direct interactions (electrostatic and/or van der Waals forces). A detailed review on the recent status of investigations concerning colloidal dispersions is given in the monographs of Russel et al. [1] and Russel [2].

The examination of concentrated colloidal dispersions, when long-range direct interactions are present, allows a wide variety of important phenomena to be studied. Information about the structure and the density of the sediment can be obtained in the case of sedimentation. The colloidal stability and coagulation phenomena in the latter could also be studied.

Another process, where direct interparticle interactions are known to be important, is membrane filtration. Much experimental evidence shows that when ultrafiltration of charged colloidal particles is performed, an anomalously high transmembrane flux (compared with the case of uncharged particles) could be observed [3–6]. This is due to the particle charge because when different species of opposite charge are filtered, a rapid decrease of the filtration rate takes place [7]. These effects have been attributed to changes both of the particle diffusivity (due to the particle charge [4]), and of the packing density in the filtration layer, formed at the membrane surface during the process [3,5,6].

*Corresponding author.
[α] Paper presented at the XII European Chemistry at Interfaces Conference, Lund, Sweden, 28 June–2 July 1992.

As a result of the electrostatic repulsion the colloidal particles are at a certain distance from each other. Different factors, however, may lead to compression of the electric double layers of the particles, thus increasing their density in the filtration layer and hence, the resistance of the latter.

The diffusivity of charged colloidal particles is also known to be a complex function of the particle volume fraction. The collective diffusion coefficient increases linearly with the volume fraction when the latter is low [8–11]. However, at a higher concentration of colloids, it starts decreasing thus passing through a maximum, as was shown theoretically by means of numerical calculations [10,11]. The derivation of an analytical expression for the collective diffusion coefficient may help elucidate the physical nature of such behavior.

Our aim in the present paper is to study some closely related problems encountered with concentrated dispersions of charged colloidal particles: (i) sediment structure with an emphasis on the coagulation phenomena; (ii) structure and permeability of the filter cake, formed in the course of ultrafiltration of such suspensions; (iii) dependence of the collective diffusion coefficient on different parameters of the colloidal dispersion.

As pointed out by Zharkikh [12], the application of rigorous statistical mechanics to transport processes in concentrated colloidal dispersions leads to such a complexity in the treatment, that as a first step, a simple cell model can be used. The cell model for describing the fluid flow in an ensemble of uncharged spherical particles, was proposed by Happel [13], Happel and Brenner [14], and Probstein [15]. It was modified recently for studying other transport phenomena, e.g. microion diffusion in concentrated dispersions of charged colloidal particles [12,16]. The cell model is known to give good quantitative results for a wide range of particle volume fractions [12,14] and is qualitatively correct for almost any concentration of colloids [12,16]. The analysis of the colloidal stability is performed in the framework of the Derjaguin–Landau–Verwey–Overbeek (DLVO) theoretical concepts [17,18]. If the applied outer force (gravitational, Brownian or viscous) on a given particle does not exceed the direct force barrier between two particles (cf. the DLVO theory) no coagulation should be observed. It is obvious that the colloidal stability problem is of great practical importance, especially in filtration, where the coagulation in the filter cake can lead to a decrease in the efficiency of the process.

The paper is organized as follows. Section 2 presents the general force balance for a given particle in the dispersion, which is the basic equation of our theoretical model; Section 3 deals with the application of this equation to the particular cases of sedimentation, ultrafiltration and diffusion of charged colloidal particles at high volume fractions; some numerical results and discussions are also included. Section 4 (Concluding remarks) summarizes our main findings.

2. Force balance on an arbitrary particle in a concentrated dispersion of charged colloidal particles

In this section we present the derivation of a general expression connecting the outer (gravitational, Brownian and/or viscous) and the direct colloidal surface forces with the local structure of the dispersion. It is based on the force balance on a given colloidal particle (see Fig. 1). Our approach is similar to the one applied by Buscall and White [19] for studying sedimentation. However, these authors performed a force balance on a certain volume of the dispersion, which contains many particles. Our choice of examining a single particle allows us to express all the quantities in which we are interested in terms of the simple pair DLVO interparticle interactions, the parameters of the hydrodynamic cell model and the local packing geometry. The main assumptions which we used are as follows. (i) The electrokinetic effects due to coupling between convection and diffusion of small ions are ignored. This means that the microion diffusion is much faster than the convection. Indeed, for convective velocities $V \approx 10^{-3}$ cm s^{-1}, ion diffusivity $D_i \approx 10^{-5}$ cm^2 s^{-1} and characteristic

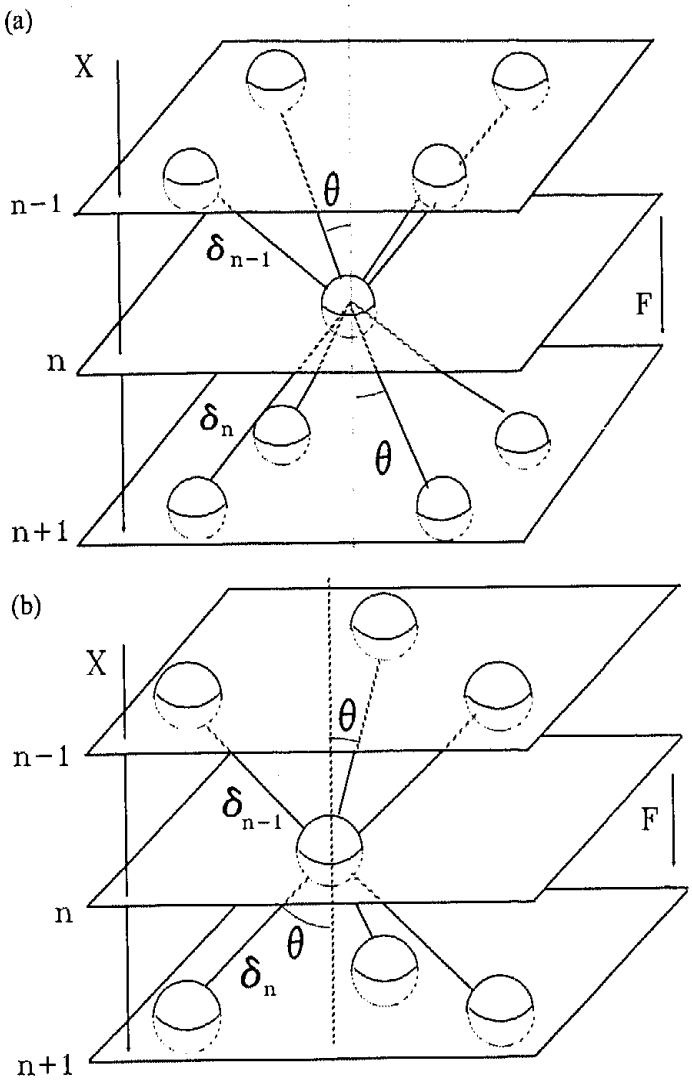

Fig. 1. Scheme of the forces acting on an arbitrary particle in a concentrated suspension: (a) body centered cubic geometry; (b) hexagonal geometry.

length of diffusion l (of the order of the particle radius $a \approx 10^{-5}$ cm), we have for the Peclet number $Pe \approx Vl/D \approx 10^{-3}$, which justifies this assumption. (ii) The force balance is performed only in a direction collinear with the outer force vector (cf. Fig. 1). Nevertheless, the variation in the particle density (due to the outer force) is assumed to take place isotropically. The meaning of this assumption will become clearer after some explanations given below. (iii) Only nearest neighbor interactions are included. (iv) Transition from discrete to continual description is used.

The system we consider is shown in Fig. 1. The distances between the chosen particle in the nth layer and its nearest neighbors in the upper $(n-1)$ and lower $(n+1)$ sublayers are δ_{n-1} and δ_n respectively. Hence, at equilibrium we obtain for the force balance:

$$\boldsymbol{F}(x_n) + m[\boldsymbol{f}(\delta_{n-1}) + \boldsymbol{f}(\delta_n)] = \boldsymbol{0} \tag{2.1}$$

where $\boldsymbol{F}(x_n)$ is the vector of the outer force which is assumed to have only an x component (the layer is considered to be infinite in the lateral directions), $\boldsymbol{f}(\delta_{n-1})$ and $\boldsymbol{f}(\delta_n)$ are the vectors of the direct (surface) forces, acting on the nth particle from the nearest neighbors in the $n-1$ and $n+1$ sublayers; m is the number of the nearest neighbors in the $n-1$ or $n+1$ sublayers, or $2m$ is the effective number of all nearest neighbors. Equation (2.1) can be written in scalar form

$$F(x_n) + m\cos\theta[f(\delta_{n-1}) - f(\delta_n)] = 0 \tag{2.2}$$

where F and f are the corresponding force magnitudes and θ is the angle between the interparticle direct force and the outer force (or the coordinate x; cf. Fig. 1 and Eq. (2.9) below). Assumption (ii) implies that δ may vary with x, but θ remains constant. This is tantamount to assuming that the local structure symmetry is not subject to great changes under the action of the outer force.

Assumption (iv) allows one to write

$$\frac{f(\delta_n) - f(\delta_{n-1})}{\delta_n - \delta_{n-1}} \frac{\delta_n - \delta_{n-1}}{x_n - x_{n-1}} \approx \frac{\partial f}{\partial x} \frac{\mathrm{d}\delta}{\mathrm{d}x} \tag{2.3}$$

where

$$x_n - x_{n-1} = [2a + \delta(x)]\cos\theta \tag{2.4}$$

and a is the particle radius. Combining the above expressions with Eq. (2.2) we obtain

$$F(x) = m\cos^2\theta[2a + \delta(x)] \frac{\partial f}{\partial \delta} \frac{\mathrm{d}\delta}{\mathrm{d}x} \tag{2.5}$$

Equation (2.5) presents the basic expression in our theoretical model. It relates the forces acting on the particle with the interparticle distances and packing geometry. It is convenient to reformulate Eq. (2.5) in the framework of the cell model [12–16]. For this purpose we introduce a new

variable γ defined as

$$\gamma^3 = \Phi, \qquad \gamma = \frac{a}{b} \tag{2.6}$$

where Φ is the particle volume fraction and $b = (4\pi a^3/3\Phi)^{1/3} = (\delta + 2a)/2\gamma_0$ is the cell radius. γ_0 corresponds to the close packing value of γ (i.e. to $\delta = 0$) for a given geometry (see Table 1). Equation (2.6) leads to

$$\left(1 + \frac{\delta}{2a}\right) = \frac{\gamma_0}{\gamma} \tag{2.7}$$

Equations (2.5) and (2.7) along with the identity

$$\frac{\partial f}{\partial \delta}\frac{\mathrm{d}\delta}{\mathrm{d}x} = \frac{\partial f}{\partial \gamma}\frac{\mathrm{d}\gamma}{\mathrm{d}x} \tag{2.8}$$

give rise to

$$F(x) = 2a\gamma_0 m \cos^2\theta \frac{1}{\gamma}\frac{\partial f}{\partial \gamma}\frac{\mathrm{d}\gamma}{\mathrm{d}x} \tag{2.9}$$

This quantity corresponds to the gradient of the elastic stress in a particulate network, introduced by Buscall and White (see Eq. (1.7) in Ref. 19).

The product

$$M = \gamma_0 m \cos^2\theta \tag{2.10}$$

characterizes the specific geometry of local ordering in the colloidal dispersion (see Fig. 1) and could be regarded as a free parameter in the interpretation of experimental data. The values for γ_0, m, and $\cos\theta$, for certain geometries are summarized in Table 1.

For the determination of the derivative $\partial f/\partial\gamma$ a specific form for the direct interaction potential is needed. Alexander et al. [20] solved numerically the non-linear Poisson–Boltzmann equation,

$$\nabla^2 y = -\frac{4\pi e^2}{\epsilon kT}\sum_i C_i z_i \exp(-z_i y) \tag{2.11}$$

for a spherical cell, surrounding the charged colloidal sphere. $y(r) = e\Psi(r)/kT$ is the dimensionless potential, kT is the thermal energy, ϵ is the dielectric constant, e is the elementary charge, C_i is the number concentration of microions of the type i and z_i is the corresponding microion charge number. They showed that the interaction energy between the sphere inside the cell and the other spheres outside the cell has a Yukawa form

$$U_{\mathrm{el}} = \frac{(ze)^2}{\epsilon}\frac{\exp(-\kappa r)}{r} \tag{2.12}$$

where r is the interparticle distance. The particle charge number z in Eq. (2.12), however, is a renormalized effective quantity [20]. It can be related to the actual particle charge by solving numerically the Poisson–Boltzmann equation (2.11) with an appropriate condition at the cell boundary [20]. The screening parameter,

$$\kappa^2 = \frac{4\pi e^2 z^2 C_0}{\epsilon kT} + \frac{4\pi e^2}{\epsilon kT}\sum z_i^2 C_i \tag{2.13}$$

also depends on the renormalized charge z. C_0 is the average particle number concentration in the suspension and C_i is the microion concentration taken at the cell boundary [20] (see also the papers of Beresford-Smith et al. [21]). The first term on the right-hand side of Eq. (2.13) accounts for the contribution of the colloidal particle counterions, while the second one is due to the added electrolyte. It is convenient to introduce the Bjerrum length,

$$\lambda = \frac{e^2}{\epsilon kT} \tag{2.14}$$

and then Eq. (2.12) becomes

$$\frac{U_{\mathrm{el}}}{kT} = z^2\lambda\frac{\exp(-\kappa r)}{r} \tag{2.15}$$

Hence the electrostatic force, acting between two

Table 1
Values of the parameters γ_0, m and $\cos\theta$ for certain packing geometries

Packing geometry	Parameter		
	γ_0	m	$\cos\theta$
Simple cubic	0.806	1	1
Body centred cubic	0.879	4	$\sqrt{3}/3$
Hexagonal	0.904	3	$\sqrt{2/3}$

particles in the dispersion, can be expressed in the following form

$$f_{el} = z^2 \lambda kT \frac{\exp(-\kappa r)}{r^2}(\kappa r + 1) \tag{2.16}$$

Using

$$r = 2a\left(1 + \frac{\delta}{2a}\right) \tag{2.17}$$

and Eq. (2.7), the electrostatic force can be expressed in terms of γ. Differentiating f_{el} with respect to γ we obtain

$$\frac{\partial f_{el}}{\partial \gamma} = \frac{z^2 \lambda kT\kappa a}{2a^2\gamma_0(2\kappa a\gamma_0/\gamma)} \exp\left(-\frac{2\kappa a\gamma_0}{\gamma}\right) \times \left[\frac{2\kappa a\gamma_0}{\gamma}\left(\frac{2\kappa a\gamma_0}{\gamma} + 1\right) + \left(\frac{2\kappa a\gamma_0}{\gamma} + 2\right)\right] \tag{2.18}$$

As discussed above, the renormalized charge z and the screening parameter κ in Eq. (2.18) differ from the actual ones. This means that they must be regarded either as free parameters in the treatment of experimental data, or the non-linear Poisson–Boltzmann equation should be taken into consideration.

For the van der Waals attractive potential between two spheres, the Hamaker equation holds [22]

$$U_{vw} = -\frac{A}{12}\left(\frac{1}{\delta/a + \delta^2/4a^2} + \frac{1}{1 + \delta/a + \delta^2/4a^2} + 2\ln\frac{\delta/a + \delta^2/4a^2}{1 + \delta/a + \delta^2/4a^2}\right) \tag{2.19}$$

where A is the Hamaker constant. Performing algebraic transformations similar to those already described above for the electrostatic part, the following expression for the van der Waals contribution can be obtained,

$$\frac{\partial f_{vw}}{\partial \gamma} = -\frac{A}{12a}\frac{\gamma^6(7\gamma_0^2 - 3\gamma^2)}{\gamma_0^3(\gamma_0^2 - \gamma^2)^3} \tag{2.20}$$

A significant simplification can be achieved in the case of large particles and high concentrations of added electrolyte. In this case the gap between the spheres is much smaller than their radius. Then, the following expressions for the interaction energies hold [1,17,18]:

$$U_{el} = 8a\epsilon\left[\frac{kT}{e}\tanh\left(\frac{y_S}{4}\right)\right]^2 \exp(-\kappa\delta) \tag{2.21}$$

and

$$U_{vw} = -\frac{A}{12}\frac{a}{\delta} \tag{2.22}$$

y_S is the dimensionless particle surface potential (cf. Eq. (2.11) and the explanations below). The force derivatives $\partial f/\partial\gamma$ are

$$\frac{\partial f_{el}}{\partial \gamma} = 16\epsilon\gamma_0\left[\kappa a\frac{kT}{e}\tanh\left(\frac{y_S}{4}\right)\exp(\kappa a)\right]^2 \times \frac{\exp(-2\kappa a\gamma_0/\gamma)}{\gamma^2} \tag{2.23}$$

and

$$\frac{\partial f_{vw}}{\partial \gamma} = -\frac{A}{12a}\frac{\gamma_0\gamma}{2(\gamma_0 - \gamma)^3} \tag{2.24}$$

Equations (2.18) and (2.20) are preferred when smaller particles with a low concentration of electrolyte are considered ($\kappa a < 1$), while (2.23) and (2.24) are correct for larger particles at high electrolyte concentration ($\kappa a > 1$).

3. Sedimentation, ultrafiltration and diffusion

In this section the approach described above is applied to examine the structure and stability of a sediment or filter cake as functions of different parameters. The time behavior of the cake permeability, when charged colloidal particles are filtered, is also investigated. After reaching the sediment (or filter cake) by means of convective transport, the particles are supposed to become motionless and all the changes in the layer structure are quasi-static. A simple expression for estimation of the collective diffusion coefficient of charged particles at relatively high volume fractions is presented.

3.1. Structure and stability of a sediment built up of charged colloidal particles

The theoretical analysis of transient settling of an uncharged hard sphere suspension was performed in a comprehensive manner by Russel et al. [1] and Davis and Russel [23]. Using the method of matched asymptotic expansions, they solved the diffusion problem for the whole region in which the settling process takes place. Some experiments with silica particles in organic solvent were also performed [24,25].

Our approach accounts for the presence of long-range direct interactions and is based on the use of Eq. (2.9). The outer force F in the case of gravity sedimentation is given by

$$F = \frac{4}{3}\pi a^3 \Delta\rho g \tag{3.1}$$

where $\Delta\rho$ is the density difference between the particles and the surrounding fluid and g is the acceleration due to gravity. The sedimentation flux for large particles (i.e. the particle convection dominates over the particle diffusion) is

$$j_{sed} = V\Phi_B \tag{3.2}$$

where Φ_B is the colloidal particle volume fraction in the bulk, above the sediment layer, and V is the *particle* sedimentation velocity in the bulk, *above* the sediment layer, in which the force balance (Eq. (2.9)) is performed. If the interparticle interactions in the bulk are ignored (the volume fraction in the bulk is low, $\Phi_B \ll 1$) and the Peclet number is high enough, V is given by the well-known expression for the gravity settling [2,23]

$$V = \frac{F}{6\pi\mu a} = \frac{2a^2\Delta\rho g}{9\mu} \tag{3.3}$$

where μ is the solvent viscosity. In our case $\Phi_B = 10^{-3}$ (see the calculations described below) and $Pe \approx 10^6$ (see Ref. 23), hence Eq. (3.3) holds. It is possible, in principle, to account for the influence of the pair interactions on the sedimentation velocity V in a rather simple manner [8,9]. However, for clarity and simplicity the interparticle interactions in the bulk are ignored in the present consideration.

We can write the following mass balance equation

$$\frac{d}{dt}\left[\int_0^{L(t)} \gamma^3(x,t)\,dx\right] = V\Phi_B \tag{3.4}$$

where t is time and $L(t)$ is the time dependent thickness of the sediment layer.

Equations (2.9), (3.1) and (3.3) give (cf. also Eq. (2.10))

$$\frac{3\pi\mu V}{M} = \frac{1}{\gamma}\frac{\partial f}{\partial \gamma}\frac{d\gamma}{dx} \tag{3.5}$$

It should be emphasized that Eq. (3.5) presents a balance between the gravity force (see Eq. (3.1)) and the interparticle force (see Eq. (2.9)) and is valid in the sediment layer only. The gravity force, however, could be expressed by the *bulk* sedimentation velocity (see Eq. (3.3) which should be applied *above* the sediment layer), which leads to the form of Eq. (3.5). If no coagulation is present in the sediment, after changing (by means of Eq. (3.5)) the variables in Eq. (3.4) we can write the latter in the following form

$$\frac{M}{3\pi\mu}\frac{d}{dt}\left[\frac{1}{V}\int_{\gamma_S}^{\gamma_L(t)} \gamma^2 \frac{\partial f}{\partial \gamma}\,d\gamma\right] = V\Phi_B \tag{3.6}$$

where γ_S is the value of γ at the surface of the sediment layer and can be calculated from the simple force balance on a particle placed there (cf. Fig. 1)

$$\frac{4}{3}\pi a^3 \Delta\rho g = m\cos\theta f(\gamma_S) \tag{3.7}$$

$\gamma_L(t)$ is the value of γ at the bottom of the sediment (where $x = L$). Equation (3.7), which presents a balance between outer and interparticle forces, shows that our approach is very similar to that of

Napper [26] for calculation of the osmotic pressure of concentrated suspensions of sterically stabilized particles. At the moment $t=0$ we assume $L=0$, $\gamma_L=\gamma_S$, i.e. the influence of the particle–membrane interactions is ignored. If there is no coagulation of the particles inside the layer, integration of (3.6) over t yields:

$$\int_{\gamma_S}^{\gamma_L(t)} \gamma^2 \frac{\partial f}{\partial \gamma} d\gamma = \frac{3\pi\mu V^2 \Phi_B}{M} t \tag{3.8}$$

which allows the calculation of the time dependence of γ_L, i.e. of the value of γ at the bottom of the layer. The spatial distribution of γ, i.e. its dependence on x, can be found from the integral of (3.5):

$$x = \frac{M}{3\pi\mu V} \int_{\gamma_S}^{\gamma(x)} \frac{1}{\gamma} \frac{\partial f}{\partial \gamma} d\gamma \tag{3.9}$$

where $\gamma(x)$ denotes the value of γ at a distance x from the surface of the layer. By substituting $\partial f/\partial\gamma$ from Eqs. (2.23) and (2.24), Eq. (3.9) can be solved to give an analytical expression for the concentration distribution along the x coordinate

$$x = \frac{M}{3\pi\mu V}\left\{8\epsilon\kappa a\left[\frac{kT}{e}\tanh\left(\frac{\gamma_S}{4}\right)\exp\kappa a\right]^2 \times\left[\frac{\exp(-2\kappa a\gamma_0/\gamma)}{\gamma} - \frac{\exp(-2\kappa a\gamma_0/\gamma_S)}{\gamma_S}\right] - \frac{A}{48a}\gamma_0\left[\frac{1}{(\gamma_0-\gamma)^2} - \frac{1}{(\gamma_0-\gamma_S)^2}\right]\right\} \tag{3.10}$$

By setting $x=L$ in Eq. (3.9) or Eq. (3.10) and making use of the value $\gamma_L(t)$, one can calculate the thickness L of the non-coagulated layer at a given moment t.

Equation (3.8) shows that as time passes, the density at the bottom of the layer γ_L^3 increases and the interparticle distance δ decreases (cf. Eq. (2.7)). As is evident from Fig. 2, the repulsive force f between the particles, which counterbalances the weight of the layer, also goes up. If however δ can attain values corresponding to the maxima of the

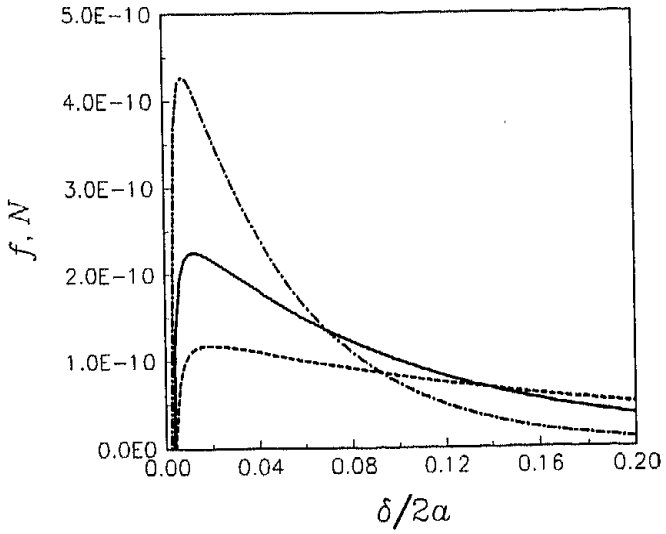

Fig. 2. Interparticle force f, acting between two colloidal spheres, according to the DLVO theory (see Eqs. (2.20) and (2.21) and the comments in text). $\Psi_S = 100$ mV; $a = 10^{-5}$ cm; $A = 10^{-20}$ J; – – –, $\kappa a = 5$; ——, $\kappa a = 10$; —·—, $\kappa a = 20$.

curves of Fig. 2, the long-range repulsive forces will no longer be able to sustain the equilibrium and the layer will collapse: at that critical moment, which we shall denote by t_{cr}, the distance between the particles will become equal to their diameter and γ will acquire the close packing value γ_0. The thickness of the non-condensed layer at the critical moment will be denoted by x_{cr} and the respective value of γ by γ_{cr}. Since the latter corresponds to the maximum of the force–distance curves, it is determined by the condition

$$\frac{\partial f}{\partial \gamma} = 0 \tag{3.11}$$

and can be calculated by means of the equations for the interaction forces, quoted in Section 2. By substituting γ_{cr} for γ_L in Eqs. (3.8) and (3.9) (or (3.10)) one can calculate also the critical time t_{cr} and the critical layer thickness x_{cr}.

After the critical moment, the thickness of the layer $L(t)$ keeps increasing but only through increasing the thickness $L - x_{cr}$ of its "condensed" part with density γ_0^3. The latter can be calculated by setting $\gamma = \gamma_0$ in Eq. (3.4) and integrating over t from t_{cr} to t. The result is

$$L(t) - x_{cr} = \frac{V\Phi_B}{\gamma_0^3}(t - t_{cr}) \tag{3.12}$$

The above procedure of calculation is applicable both to gravity and centrifugal sedimentation. In the former case in all equations V must be expressed through the second Eq. (3.3), which is valid also for the latter case if the centrifugal acceleration is substituted for g.

The calculated concentration profiles in the sediments are shown in Fig. 3. The sedimentation of particles with radius $a = 5 \times 10^{-5}$ cm and density difference $\Delta\rho = 0.8$ under the gravity force is considered. Figure 3(a) corresponds to the case of body centered cubic geometry ($\gamma_0^3 = 0.8794$, or maximal volume fraction $\Phi_0 = 0.68$) of particles with surface potential $\Psi_S = 100$ mV. The curves correspond to three different concentrations of electrolyte: $\kappa a = 5$, 10 and 20 respectively. In the case where $\kappa a = 5$ and with body centered cubic geometry at the sedimentation layer surface ($x = 0$), $\gamma_S = 0.4176$ (cf. Eq. (3.7)) and coagulation occurs at $\gamma_{cr} = 0.8717$ ($x_{cr} = 4.3$ cm) (cf. Eqs. (3.10) and (3.11)). This means that after building a sediment with height equal to 4.3 cm, the particles placed in the nearest two sublayers to the membrane will coagulate (cf. Fig. 1). The increase of the electrolyte concentration leads to an increase of the surface density of particles ($\gamma_S = 0.5606$ for $\kappa a = 10$ and $\gamma_S = 0.6867$ for $\kappa a = 20$). Also, the change in the particle volume fraction (i.e. of γ) with the coordinate x is steeper for higher electrolyte concentrations (see Fig. 3). The coagulation occurs at larger values of x and γ. Thus for $\kappa a = 10$ and body centered cubic packing ($\gamma_0 = 0.8794$) we obtained $x_{cr} = 7.9$ cm and $\gamma_{cr} = 0.8745$,

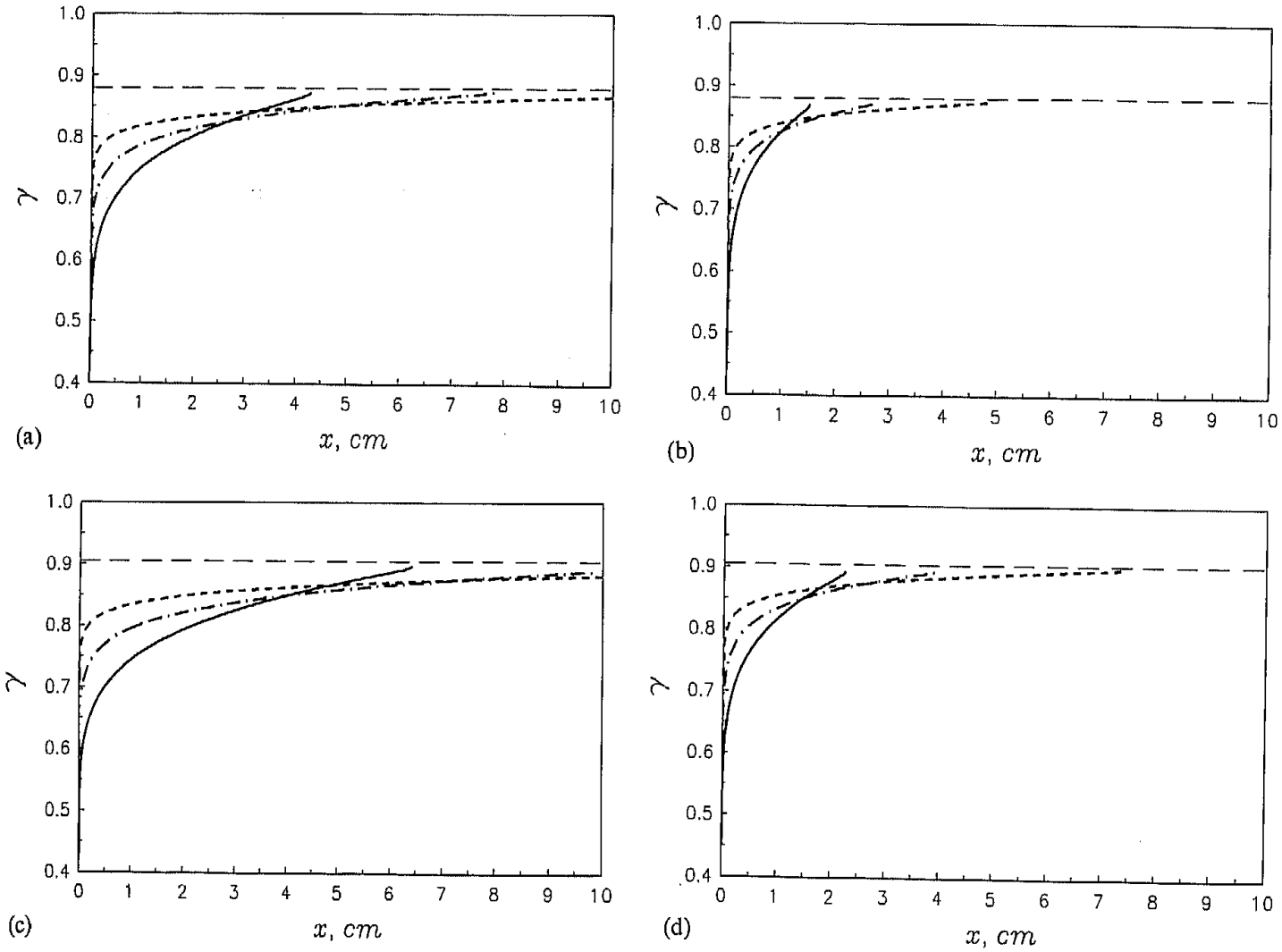

Fig. 3. Concentration distribution of charged colloidal particles in a sedimentation layer under the force of gravity; $x = 0$ corresponds to the surface of the layer. $a = 5 \times 10^{-5}$ cm; $\Delta\rho = 0.8$; $A = 10^{-20}$ J; ——, $\kappa a = 5$; —·—, $\kappa a = 10$; – – –, $\kappa a = 20$. (a) $\Psi_S = 100$ mV, body centered cubic geometry; (b) $\Psi_S = 50$ mV, body centered cubic geometry; (c) $\Psi_S = 100$ mV, hexagonal geometry; (d) $\Psi_S = 50$ mV, hexagonal geometry. The horizontal dashed lines correspond to γ_0 (see Table 1).

while for $\kappa a = 20$ no coagulation takes place for $x \leqslant 10$ cm (in this case $x_{cr} = 14.6$ cm and $\gamma_{cr} = 0.8763$). These specific features of the coagulation in the sediment are connected with the type of DLVO potential used — see Eqs. (2.21) and (2.22) and Fig. 2. It implies that addition of electrolyte moves the force maximum toward smaller interparticle distances, but increases its height. Such a situation is adequate in cases where the surface potential is constant and the particle curvature effects are unimportant. An increase of the force maximum with the electrolyte concentration for flat surfaces has been observed experimentally [27].

However, we should admit that the electrostatic energy expression we used (see Eq. (2.21)) is not strictly applicable in the whole region of particle volume fraction covered in Fig. 3. According to Derjaguin et al. [17], Eq. (2.21) is accurate for $\delta/a \leqslant 1$ and $\kappa\delta \geqslant 2$. Hence, for $\delta/a \geqslant 1$ and body centered cubic geometry of ordering (in our case this means $\gamma \leqslant 0.5863$ — see Eq. (2.7)) one should use a Yukawa (or Debye–Hückel) type of potential (i.e. Eqs. (2.12), (2.15) and (2.16)), which contains a renormalized charge number z [20,21]. For the case of high volume fractions (small interparticle distances) the situation is even more complex. The weak diffuse layer overlap condition $\kappa\delta \geqslant 2$ (which is necessary for Eq. (2.21) to be valid) requires $\gamma \leqslant 0.7328$ for $\kappa a = 5$, $\gamma \leqslant 0.7995$ for $\kappa a = 10$ and $\gamma \leqslant 0.8375$ for $\kappa a = 20$ (cf. Eq. (2.7)) and is obviously violated for certain parts of the curves in Fig. 3.

In order to check to what extent our results will be valid at small separations and high surface potentials we performed calculations by making use of the expressions for the energy and force of interaction between spherical particles proposed by Derjaguin et al. [17,18]. We found that the values for γ_{cr} calculated in this way differ by no more than 0.13% from our result. This supports the applicability of Eqs. (2.21) and (2.23).

3.2. *Structure and stability of a filter cake built up by charged colloidal particles*

The approach described and applied above to sedimentation can be used also for studying filter cake formation and coagulation during filtration. Although most of the equations are formally the same, the meaning of some quantities and thus certain physical considerations are different, in particular the following.

(i) The mass balance equation (Eq. (3.4)) is again valid, but now V, instead of being the particle sedimentation velocity, will denote the flow velocity of the liquid. The latter carries, by convection, the particles toward the membrane, thus creating a convective flux $V\Phi_B$. In the filtration case we do not employ an independent equation, like Eq. (3.3) for calculating V, because the flow velocity usually changes with time as a function of the particle layer thickness and structure: hence, it must be either taken from the experiment or calculated in the framework of the model.

(ii) All equations from Section 2 are applicable and our treatment is based again on the force balance equation (Eq. (2.9)). However, the outer force in this case is due to the viscous flow pressing the particles toward the membrane and each other. Following Refs. 13–15, we express this force in the form:

$$F = 4\pi\mu a V \varphi(\gamma) \tag{3.13}$$

where $\varphi(\gamma)$ is the Happel function

$$\varphi(\gamma) = \frac{3 + 2\gamma^5}{2 - 3\gamma + 3\gamma^5 - 2\gamma^6} \tag{3.14}$$

F is the resistance force, acting on the fluid flowing through an assemblage of motionless particles, with *superficial* velocity V [14,15].

An alternative and simpler expression which might be useful in some cases for $\varphi(\gamma)$ can be obtained by using the Kozeny–Carman model [14,15]. Darcy's equation in the framework of the Kozeny–Carman theory reads (P is the applied pressure)

$$V = \frac{4a^2(1-\gamma^3)^3}{180\gamma^6\mu}\frac{dP}{dx} \tag{3.15}$$

The drag force is

$$F = \frac{4}{3}\pi\frac{a^3}{\gamma^3}\frac{dP}{dx} \tag{3.16}$$

Eliminating dP/dx between these two equations and comparing the result with Eq. (3.13) one sees that the function

$$\varphi_{kc}(\gamma) = 15\left(\frac{\gamma}{1-\gamma^3}\right)^3 \tag{3.17}$$

is the Kozeny–Carman analog of Eq. (3.14). Equations (3.14) and (3.17) are compared below.

Comparing Eqs. (3.13) (cf. also (3.14)) with the first Eq. (3.3) one sees that the same results as for sedimentation will hold provided that $(\frac{2}{3})V\varphi(\gamma)$ is substituted for V in the equations involving force balance. Note however that $\varphi(\gamma)$ must remain under the sign of the integral. Thus, the counterparts of Eqs. (3.6), (3.8) and (3.9) now become:

$$\frac{d}{dt}\left[\frac{M}{2\pi\mu V}\int_{\gamma_S(t)}^{\gamma_L(t)}\frac{\gamma^2}{\varphi(\gamma)}\frac{\partial f}{\partial\gamma}\,d\gamma\right] = V\Phi_B \tag{3.18}$$

and

$$\frac{M}{2\pi\mu V\Phi_B}\int_{\gamma_S(t)}^{\gamma_L(t)}\frac{\gamma^2}{\varphi(\gamma)}\frac{\partial f}{\partial\gamma}\,d\gamma = \int_0^t V\,dt' \tag{3.19}$$

$$x = \frac{M}{2\pi\mu V}\int_{\gamma_S(t)}^{\gamma}\frac{1}{\varphi(\gamma)\gamma}\frac{\partial f}{\partial\gamma}\,d\gamma \tag{3.20}$$

The surface value $\gamma_S(t)$ in the above equation was found by using the theory of Sherwood [28], who calculated the viscous force acting on a sphere placed on a semipermeable half space (i.e. membrane with infinite thickness). For the force balance of a particle, placed at the filtration layer surface, we thus obtained

$$6\pi\mu a V 0.645 = m\cos\theta f(\gamma_S) \tag{3.21}$$

which is the counterpart of Eq. (3.7). Our estimates showed that the dependence of γ_S on time is very weak and in the future we shall neglect it.

The hydrodynamic drag force, just like the gravity force, tends to compress the particle layer, so that again at a given moment t_{cr} coagulation can occur. The critical value γ_{cr} is again determined by Eq. (3.11) and the respective time t_{cr} and thickness x_{cr} are calculated from Eqs. (3.19) and (3.20) with γ_{cr} substituted for γ_L. The thickness of the coagulated layer $L - x_{cr}$ depends on time as (cf. Eq. (3.12))

$$L - x_{cr} = \frac{\Phi_B}{\gamma_0^3}\int_{t_{cr}}^{t} V(t')\,dt' \tag{3.22}$$

In order to calculate the dependence of the filtration velocity V on time (which incidentally is of major interest in membrane science and technology) we used the Darcy equation in the form

$$V = \frac{\Delta P}{(1/k_0)+(1/k_F)} \tag{3.23}$$

where ΔP is the pressure drop, the constant k_0 is the membrane permeability and k_F is the filtration layer permeability which can be expressed through the function φ and γ by means of the equation [1,2]:

$$k_F = \frac{a^2}{3\mu\int_0^{L(t)}\varphi\gamma^3\,dx} \tag{3.24}$$

Taking into account Eqs. (2.9), (3.13), (3.14) and (3.24), we obtained for our model *before coagulation*:

$$k_F = \frac{2\pi a^2 V}{3M\int_{\gamma_S(t)}^{\gamma_L(t)}\gamma^2\frac{\partial f}{\partial\gamma}\,d\gamma} \tag{3.25}$$

Introducing Eq. (3.25) into Eq. (3.23), after simple calculations we can derive an expression for the velocity change with time:

$$V(t) = V_0 - \frac{3k_0 M}{2\pi a^2}\int_{\gamma_S(t)}^{\gamma_L(t)}\gamma^2\frac{\partial f}{\partial\gamma}\,d\gamma \tag{3.26}$$

where

$$V_0 = k_0\Delta P \tag{3.27}$$

is the flow velocity at moment $t = 0$, when no filter

cake is present. After coagulation has occurred, an additional term $1/k_F^c$ which accounts for the contribution of the coagulated part of the layer should be added in the denominator of (3.23),

$$k_F^c = \frac{a^2}{3\mu\varphi(\gamma_0)\gamma_0^3(L - x_{cr})} \tag{3.28}$$

being the permeability of the condensed layer (cf. Eq. (3.24)). After simple calculations, an expression accounting for both the flocculated and non-flocculated parts is derived

$$V(t) = \frac{V_0 - \dfrac{3k_0 M}{2\pi a^2}\displaystyle\int_{\gamma_{S(t)}}^{\gamma_{cr}} \gamma^2 \frac{\partial f}{\partial \gamma}\,d\gamma}{1 + \dfrac{3k_0\mu}{a^2}\varphi(\gamma_0)\gamma_0^3[L(t) - x_{cr}(t)]} \tag{3.29}$$

Hence, the decrease in the filtration rate with time is due both to the non-flocculated part (the second term in the numerator in Eq. (3.29)) and to the flocculated part (the second term in the denominator in Eq. (3.29)) of the filtration layer.

We now have available a set of equations for the calculation of all quantities of interest. In Fig. 4, the concentration distribution of the particles in the layer is shown. The curves in Fig. 4(a) are for constant filtration velocity $V = 10^{-3}$ cm s^{-1}, and reveal the influence of the electrolyte concentration (or κa). The assumed packing geometry is body centered cubic, and the particle surface potential is 100 mV and radius $a = 10^{-5}$ cm. Comparing with the case of sedimentation (cf. Fig. 3(a)), one can see that the coagulation in the layer occurs at much smaller values of x_{cr} (about 3 orders of magnitude lower). The viscous force, however, which corresponds to $V = 10^{-3}$ cm s^{-1} is about 10^5 times greater than that due to gravity settling for the particle parameters described above. Besides, in the case of sedimentation, the higher the electrolyte concentration was, the higher the value of x_{cr} obtained. Such conformity is not present when filtration of colloidal particles is considered. The reason is that the viscous force is a strong function of γ (see Eqs. (3.13) and (3.14)) and could overcome even high interparticle force

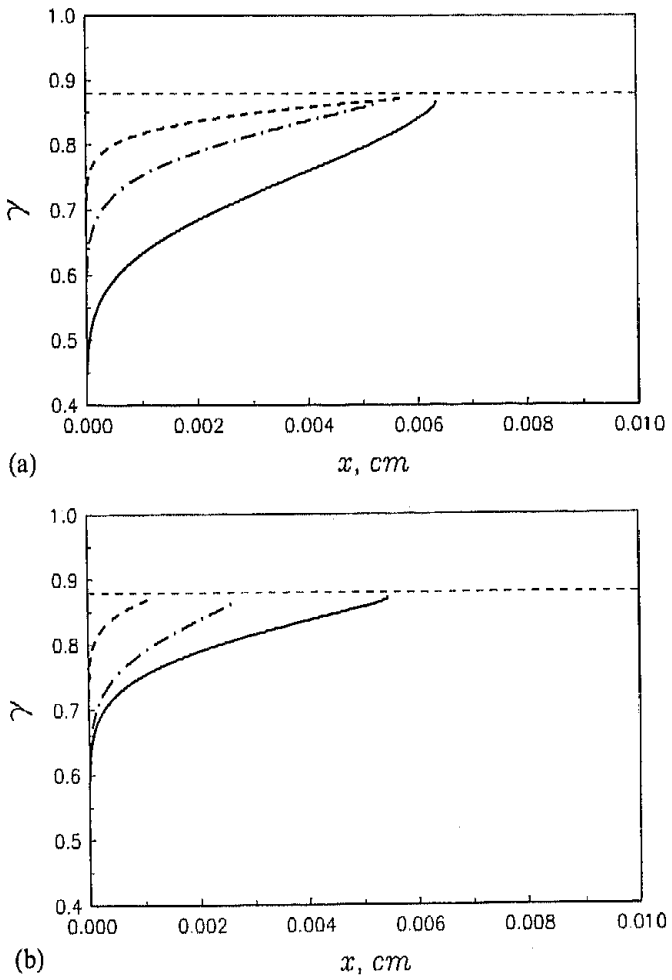

Fig. 4. Concentration distribution of charged colloidal particles in a filter cake. $a = 10^{-5}$ cm; $\Psi_S = 100$ mV; $A = 10^{-20}$ J. (a) $V = 10^{-3}$ cm s^{-1}; ——, $\kappa a = 5$; —·—, $\kappa a = 10$; – – –, $\kappa a = 20$. (b) $\kappa a = 10$; ——, $V = 10^{-3}$ cm s^{-1}; —·—, $V = 2 \times 10^{-3}$ cm s^{-1}; ---, $V = 5 \times 10^{-3}$ cm s^{-1}. The horizontal dashed lines correspond to γ_0 (see Table 1).

barriers (cf. Fig. 2) when the particle volume fraction exceeds a certain value. The influence of the outer force magnitude (i.e. the velocity V, see Eq. (3.13)), however, qualitatively resembles the sedimentation case. The greater the force is, the smaller the value for the critical layer thickness x_{cr} derived — see Fig. 4(b). All considerations concerning the applicability of Eqs. (2.23) and (2.24) in the vicinity of γ_{cr} remain the same as in the case of sedimentation (see the previous subsection).

The influence of the electrolyte on the gel layer permeability is shown in Fig. 5. The calculations are based on Eq. (3.25) which means that only the non-flocculated part is considered. Three different concentrations of electrolyte ($\kappa a = 5$, 10 and 20)

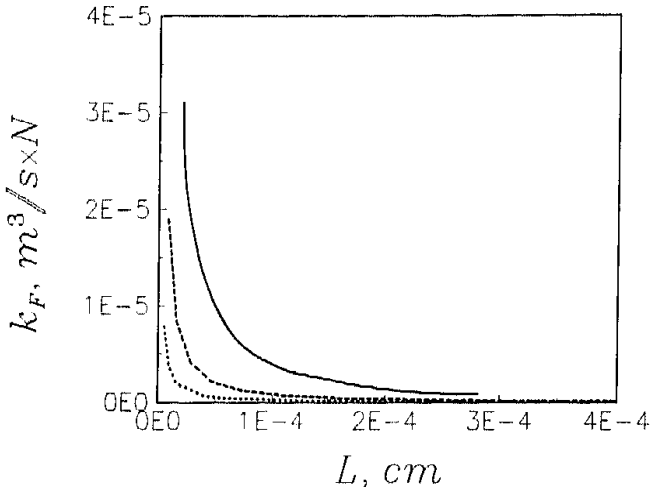

Fig. 5. Change in the filtration layer permeability with the layer thickness for different concentrations of electrolyte. ——, $\kappa a = 5$; – – –, $\kappa a = 10$; · · · · ·, $\kappa a = 20$.

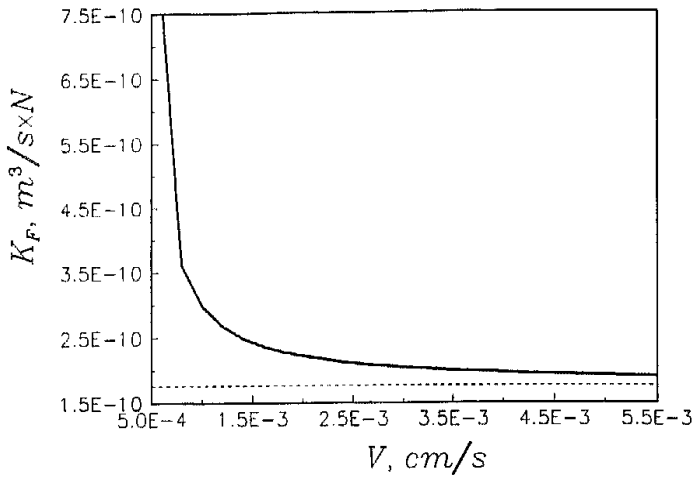

Fig. 6. Filtration layer permeability vs. filtration rate. The full curve corresponds to a layer consisting of charged particles while the dashed curve is for uncharged hard spheres. $\kappa a = 10$; $a = 10^{-5}$ cm; $\Psi_S = 100$ mV; $A = 10^{-20}$ J; $L = 10^{-2}$ cm; body centered cubic ordering is assumed.

were examined. The particle radius was assumed to be 10^{-5} cm, the surface potential $\Psi_S = 100$ mV, the Hamaker constant $A = 10^{-20}$ J and the packing geometry was body centered cubic. It is seen that the greater the electrolyte concentration, the less permeable the layer. The results are in agreement with those for the concentration profiles in the filtration layer (see Fig. 4). After coagulation, the permeability is not sensitive toward the microion content and is equal to that for uncharged hard spheres [29,30] (cf. Eq. (3.28)). It can not be plotted on the same scale in Fig. 5 because it is much too small.

Another parameter which can be expected to influence the filtration layer permeability is the filtration rate. By increasing the latter the layer becomes more compressed and hence less permeable. This is illustrated in Fig. 6. The values of the parameters are the same as in the previous figure. The curve is calculated at constant filtration layer thickness $L = 10^{-2}$ cm which can be achieved in practice by means of intensive turbulent stirring or in a cross-flow mode of operation. The filtration layer permeability sharply decreases with increasing filtration rate, tending to the value for uncharged hard spheres, shown with the dashed line. The flocculation effects taking place in the layer have been accounted for (see Eqs. (3.25) and (3.28)).

The dependence of the filtration layer permeability on the surface potential is shown in Fig. 7. Against $L = 10^{-2}$ cm, $a = 10^{-5}$ cm, $\kappa a = 10$, $A = 10^{-20}$ J, $V = 10^{-3}$ cm s^{-1} and body centered cubic geometry is assumed. The calculations are based on Eqs. (3.25) and (3.28). The layer permeability increases with the surface potential due to the increase in the interparticle repulsion. Above a certain value of the surface potential, however, the permeability reaches saturation, corresponding to an asymptotical value $k_F = 6.2 \times 10^{-9}$ cm^3 s^{-1} dyn^{-1}.

In Fig. 8 the change in the filtration layer permeability with the particle radius is shown. All the

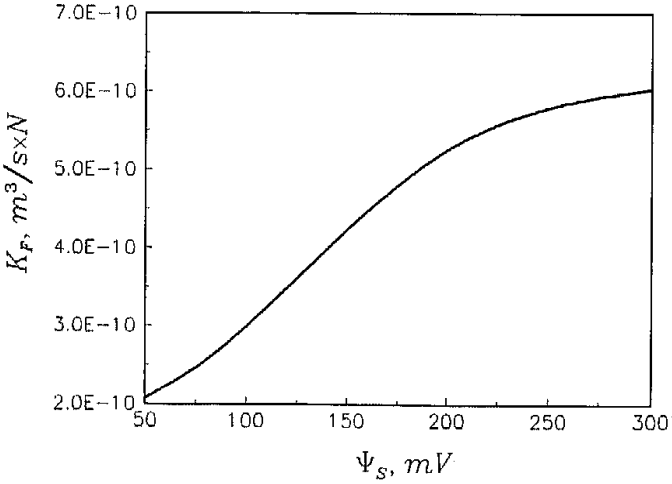

Fig. 7. Filtration layer permeability vs. surface potential. The values of the other parameters are the same as in Fig. 6.

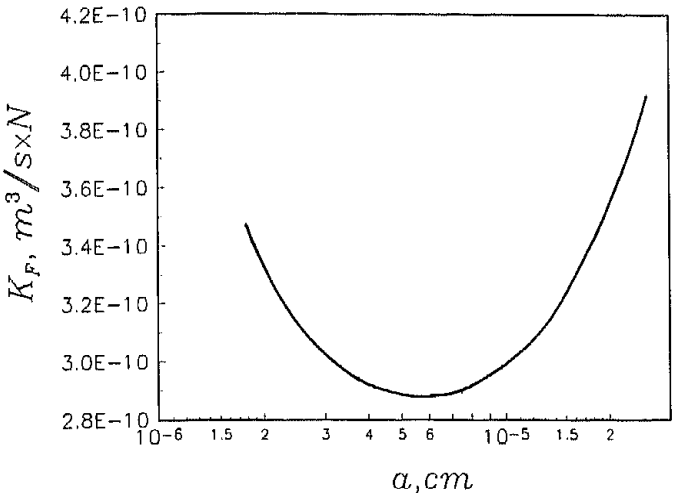

Fig. 8. Filtration layer permeability vs. particle radius; $1/\kappa = 10^{-6}$.

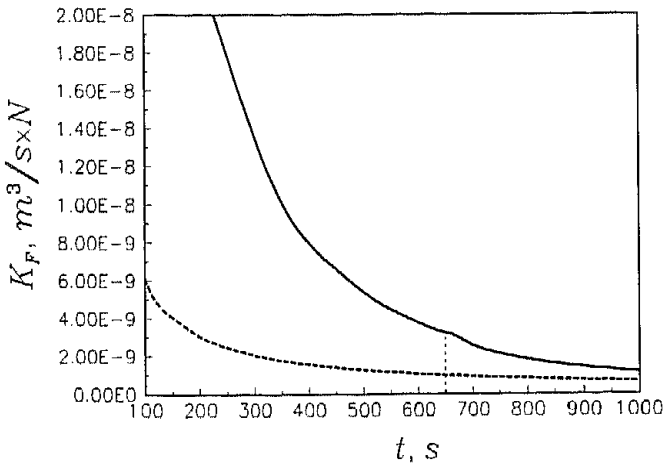

Fig. 9. Filtration layer permeability vs. time. $\kappa a = 10$; $a = 10^{-5}$ cm; $\Psi_S = 100$ mV; $A = 10^{-20}$ J; body centered cubic ordering is assumed. The full curve corresponds to the case of charged particles and the dashed one to uncharged hard spheres.

parameters are the same as above. The electrolyte concentration assumed provides a Debye screening length $1/\kappa = 10^{-6}$ cm. It is seen that the filtration layer permeability passes through a minimum with the increase of the particle radius. The minimum is around $\kappa a = 1$. The reason for such behavior in our model is that for very small particles the void fraction in the layer is great because of the dominating contribution of the interparticle spacing (due to the electrostatic repulsion). However, with the increase of the particle dimensions the fraction of solid increases and the contribution of the void volume due to the repulsive interactions becomes less significant. After a certain value of the particle radius, the electrostatic contribution becomes negligible and the layer starts to behave as if built up by uncharged hard spheres, but it is known from the filtration theories for such systems [14,15] that the permeability increases with the square of the particle radius. That is why after a given value of the particle dimensions, the layer permeability starts to increase again. A very similar dependence of the filtration layer permeability on the radius of the colloidal particles subjected to filtration was observed by Fane [31]. His explanation, however, was different and was based on the counterbalance of the Brownian diffusion (dominating for smaller particles) and particle migration due to hydrodynamic forces (dominating for larger particles). We believe that for charged particles probably both effects are present.

Figure 9 presents the case of filtration in an unstirred batch cell. In this case the filtration layer does not have constant thickness because of accumulation of particles at the membrane surface. The change of the filtration layer permeability shown in the figure is due both to change of the layer structure (e.g. compression) and its thickness. The curve was calculated by using Eqs. (3.25), (3.28) and (3.29). The suspension parameters are the same as above. The initial filtration rate V_0 was assumed to be 2×10^{-3} cm s^{-1}. The full curve is for charged colloidal particles, the dashed line is for uncharged particles, while the small vertical dashed line indicates the moment at which coagulation appears in the layer. Hence, by optimizing the filtration rate and duration of the process one can avoid the coagulation of particles at the membrane surface.

Finally a comparison between the Happel (Eq. (3.14)) and Kozeny–Carman (Eq. (3.17)) models is performed in Fig. 10. It is seen that for $\Psi_S = 100$ mV, $a = 10^{-5}$ cm, $A = 10^{-20}$ J, $\kappa a = 10$, and $V = 10^{-3}$ cm s^{-1} the two models give very similar results.

3.3. *Collective diffusion in concentrated suspension of charged colloidal particles*

In this subsection we study suspensions more dilute than the sedimentation or filtration cakes

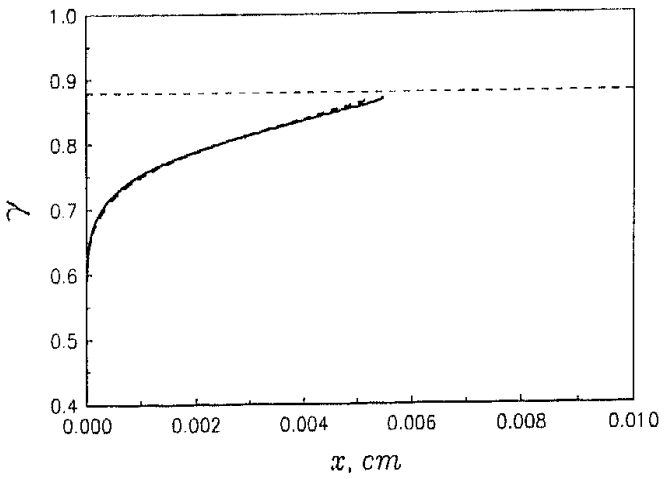

Fig. 10. Influence of the type of hydrodynamic function $\varphi(\gamma)$ on the concentration profile in a filter cake. $\Psi_S = 100$ mV; $a = 10^{-5}$ cm; $A = 10^{-20}$ J; $\kappa a = 10$; $V = 10^{-3}$ cm s^{-1}; ——, Happel model (Eq. (3.20)); – – –, Kozeny–Carman model (Eq. (3.23)). The horizontal dashed line corresponds to γ_0 (see Table 1).

treated above. Still, the considered particle volume fractions exceed those at which simple theories [8,9] (accounting only for pair interactions) could be applied. Since the particle volume fractions Φ of interest to us are lower than 0.20 (i.e. $\gamma \leqslant 0.58$), the electrostatic potential, proposed by Alexander et al. [20] can be used (see Eq. (2.18)). The van der Waals attractive interactions are ignored in the present consideration because of the relatively large interparticle distances.

The difference between the present treatment of diffusion of charged particles and the sedimentation process studied in Section 3.1 is that (i) the particles are supposed to be small enough to perform Brownian motion, and (ii) the hydrodynamic drag force is represented not by the Stokes equation (Eq. (3.3)), referring to a single particle, but by Happel's equation (Eq. (3.14)), which takes into consideration also the hydrodynamic interactions in the ensemble of particles. Thus, the total outer force $\boldsymbol{F}$ acting on a sphere, moving with velocity V in the suspension, in this case is a superposition of the Brownian force and the viscous drag:

$$\boldsymbol{F} = -\frac{kT}{\Phi}\nabla\Phi + 4\pi\mu a\varphi(\gamma)V \tag{3.30}$$

Combined with Eq. (2.9), the above expression gives the condition for steady motion of the particle

$$\frac{kT}{\Phi}\nabla\Phi + 2aM\frac{1}{3\gamma^3}\frac{\partial f}{\partial\gamma}\nabla\Phi = 4\pi\mu a\varphi(\gamma)V \tag{3.31}$$

Again, the geometrical parameters γ_0, m, $\cos\theta$ account for the local ordering. Equation (3.31) defines the velocity of motion V of the particles in the direction of the concentration gradient $\nabla\Phi$. The corresponding particle flux is:

$$j = -V\Phi \tag{3.32}$$

It can be represented also by Fick's first law:

$$j = -D_c\nabla\Phi \tag{3.33}$$

where D_c is the collective coefficient. Equating (3.32) and (3.33) and making use of Eq. (3.31), we thus obtain:

$$\frac{D_c}{D_0} = \frac{3}{2\varphi(\gamma)}\left(1 + \frac{2aM}{3kT}\frac{\partial f}{\partial\gamma}\right) \tag{3.34}$$

where

$$D_0 = \frac{kT}{6\pi\mu a} \tag{3.35}$$

is the Stokes–Einstein expression [32]. For the function $\varphi(\gamma)$, accounting for the hydrodynamic interactions, it is appropriate to use, in the case of diffusion, either the expression given by Happel [13] (see Eq. (3.14)) or the empirical relation [1,2,23]:

$$\varphi = \frac{3}{2}(1-\gamma^3)^{-6.55} \tag{3.36}$$

Both expressions for φ reduce Eq. (3.13) to Stokes law at infinite dilution (γ^3 or $\Phi \to 0$).

The ratio (3.34) is plotted in Fig. 11 as a function of Φ (or γ^3). The hydrodynamic function $\varphi(\gamma)$ is expressed by Eq. (3.14) (Fig. 9). Body centered cubic packing was assumed while the parameters of the particles are the same as in the paper of D'Aguanno et al. [10] ($a = 2.5 \times 10^{-7}$ cm, $z_0 = 20$). The calculation of the particle surface potential Ψ_S from the real surface charge z_0, for the same system, using the non-linear Poisson–Boltzmann equation, was

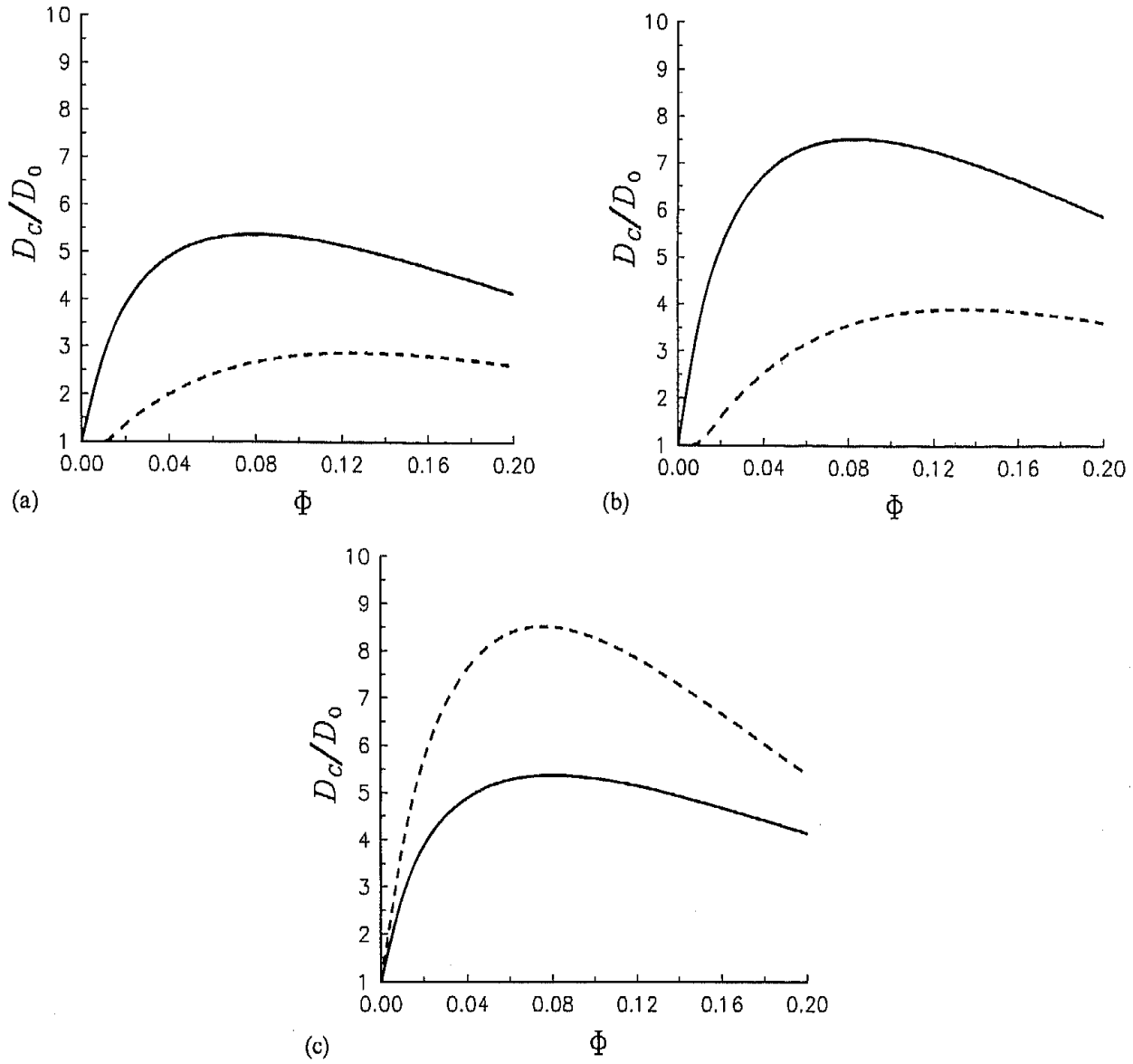

Fig. 11. Concentration dependence of the collective diffusion coefficient. $\Psi_s = 100$ mV, $a = 10^{-5}$ cm; ——, $\kappa a = 0.2626$; – – –, $\kappa a = 0.5872$; (a) body centered geometry; (b) hexagonal geometry, Happel model (Eq. (3.14)); ——, $\kappa a = 0.2626$; – – –, $\kappa a = 0.5872$; (c) body centered geometry, $\kappa a = 0.2626$; ——, Happel model (Eq. (3.14)); – – –, Eq. (3.36).

described in detail elsewhere [9]. For $\kappa a = 0.2626$, the collective diffusion coefficient initially increases with Φ, due to the interparticle repulsion, but above $\Phi \approx 0.08$ starts decreasing. This behavior resembles the result of D'Aguanno et al. [10], but these authors predicted (by exact numerical calculations) a plateau region, above a certain concentration which cannot be obtained using our approximate model. For higher electrolyte concentrations ($\kappa a = 0.5872$), the ratio D_c/D_0 is smaller, as it should be due to the decreased interparticle interaction. The fact that the curve gives $D_c/D_0 = 1$ at $\Phi = 0.015$ is probably due to the breakdown of this simple model. However, for this concentration range, accurate linear (with respect to Φ) theories are available [8,9].

The influence of the geometry of local ordering is illustrated in Fig. 11(b). All the parameters used are the same as in Fig. 11(a), but the ordering geometry is assumed to be hexagonal. The observed increase of the collective diffusion coefficient D_c with the particle volume fraction Φ (as compared with Fig. 11(a)) is due to the stronger electrostatic interparticle repulsion in the case of hexagonal geometry compared to the body centered cubic.

The role of the particular choice of the form of the hydrodynamic function $\varphi(\gamma)$ is illustrated in Fig. 11(c). The model of Happel [13–15] (see Eq. (3.14)) is compared with Eq. (3.36) [1,2,23]. It can be seen that the semiempirical expression (3.36) corresponds to lower hydrodynamic resistance, and to considerably stronger diffusion than predicted by using Eq. (3.14).

Concluding remarks

In the present paper we studied some aspects of sedimentation, ultrafiltration and diffusion in concentrated suspensions of charged colloidal particles. The approach we used is based on the force balance, performed on a given particle in the suspension (see Eq. (2.9)). It introduces, however, a presumption for the particular geometry of ordering of the particles in the suspension. Two types of geometries were examined: body centered cubic and hexagonal. They were chosen because their volume fractions of closest packing $\Phi = 0.68$, and $\Phi = 0.76$ are very close to the experimentally observed values [23,24]. Using the formulas obtained (Eqs. (2.9), (2.23), (2.24), (3.5), (3.7) and (3.8)–(3.10)), we derived the concentration distribution of charged particles in a sedimentation layer. The influence of different parameters (surface potential of the particles Ψ_S, electrolyte concentration, i.e. κa, and type of packing geometry) was studied (Fig. 3).

The critical values of the sedimentation layer thickness x_{cr}, and time t_{cr} of coagulation were also calculated for different values of the parameters. The applicability of the approximate expression for the electrostatic energy of interaction (Eqs. (2.21)–(2.24)) was discussed and comparison with other theoretical models [17,18] was presented. It was shown that Eqs. (2.21)–(2.24) can be used without introducing significant inaccuracy.

The ultrafiltration of charged colloidal particles was investigated in a similar manner. An important difference, in comparison with sedimentation, is that the outer viscous force is much greater compared to the gravity, and is volume fraction dependent. The concentration profiles in a filter cake were obtained using Eqs. (3.10), (3.11), (3.19)–(3.29) and are shown in Fig. 4. The increase of the viscous force has the same qualitative effect on the critical value x_{cr}, as the increase of the sedimentation force in the previous case (cf. Fig. 4(b)). A comparison between the cell model of Happel [13–15] and that of Kozeny–Carman [14,15] was performed (cf. Eqs. (3.14) and (3.17)). A very good agreement between both models was obtained (see Fig. 10).

The permeability of a filtration layer built up of charged colloidal particles was studied using Eqs. (3.25) and (3.28). It was shown that by increasing the electrolyte concentration one can decrease the permeability and vice versa (see Fig. 5). The filtration rate also affects the filtration layer properties. The greater the rate, the smaller the permeability (Fig. 6). The influence of the particle surface potential was also studied. Higher surface potentials lead to greater permeabilities due to the increase of the interparticle repulsion. However, above a certain value of the surface potential, a plateau value for the permeability is reached (see Fig. 7). The change of the filtration layer permeability with the particle radius passes through a minimum (see Fig. 8). Similar behavior was observed previously [31], but explained by different arguments. The change of the permeability with time in an unstirred batch cell was investigated (Fig. 9); the observed decrease is due to changes in both the layer thickness and structure.

A simple formula for the collective diffusion coefficient of charged colloidal particles at relatively high volume fraction was derived (see Eq. (3.34)). The concentration dependence of the collective diffusion coefficient passes through a maximum, due to the competition between the repulsive direct interactions and the hydrodynamic drag forces (see Figs. 11(a)–11(c)). Qualitatively, similar behavior was obtained for uncharged hard spheres [11] as well as for charged particles [10].

Acknowledgments

We are indebted to Dr. K. Danov for helpful discussions. This work was financially supported by the Bulgarian Ministry of Science and Higher Education.

References

1 W.B. Russel, D.A. Saville and W.R. Schowalter, Colloidal Dispersions, Cambridge University Press, Cambridge, 1989.
2 W.B. Russel, The Dynamics of Colloidal Systems, University of Wisconsin Press, Madison, WI, 1987.
3 R.M. McDonough, C.J.D. Fell and A.G. Fane, J. Membr. Sci., 21 (1984) 285.
4 R.M. McDonough, A.G. Fane and C.J.D. Fell, J. Membr. Sci., 43 (1989) 69.
5 M.T. Brunelle, Desalination, 32 (1980) 127.
6 D.E. Potts, R.G. Ahlert and S.S. Wang, Desalination, 36 (1981) 235.
7 G.B. Van den Berg and C.A. Smolders, J. Membr. Sci., 47 (1989) 1.
8 D.N. Petsev and N.D. Denkov, J. Colloid Interface Sci., 149 (1992) 329.
9 N.D. Denkov and D.N. Petsev, Physica A, 183 (1992) 462.
10 B. D'Aguanno, U. Genz and R. Klein, J. Phys. B., Condens. Matter, 2 (1990) 379.
11 A.B. Glendinning and W.B. Russel, J. Colloid Interface Sci., 89 (1982) 124.
12 N.I. Zharkikh, Thesis, Ukraine Academy of Sciences, Kiev, 1982.
13 J. Happel, AIChE J., 4 (1958) 197.
14 J. Happel and H. Brenner, Low Reynolds Number Hydrodynamics, Prentice Hall, Englewood Cliffs, NJ, 1965, Chapter 9.
15 R.F. Probstein, Physicochemical Hydrodynamics, Butterworths, London, 1989, Chapter 8.
16 J.B. Borkovskaya, Thesis, Ukraine Academy of Sciences, Kiev, 1987.
17 B.V. Derjaguin, N.V. Churaev and V.M. Muller, Surface Forces, Nauka, Moscow, 1985 (in Russian).
18 B.V. Derjaguin, Theory of Stability of Colloids and Thin Films, Plenum Press, New York, 1989.
19 R. Buscall and L.R. White, J. Chem. Soc. Faraday Trans., 83 (1987) 873.
20 S. Alexander, P.M. Chaikin, P. Grant, G.J. Morales and P. Pincus, J. Chem. Phys., 80 (1984) 5776.
21 B. Beresford-Smith, D.Y.C. Chan and D.J. Mitchell, J. Colloid Interface Sci., 105 (1985) 216.
B. Beresford-Smith and D.Y.C. Chan, Faraday Discuss. Chem. Soc., 76 (1983) 65.
22 H.C. Hamaker, Physica, 4 (1937) 1058.
23 K.E. Davis and W.B. Russel, Phys. Fluids A, 1 (1989) 82.
24 K.E. Davis, W.B. Russel and W.J. Glantschnig, Science, 221 (1989) 507.
25 F.M. Auzerais, R. Jackson, W.B. Russel and W.F. Murphy, J. Fluid Mech., 221 (1990) 213.
26 D.H. Napper, Polymeric Stabilization of Colloidal Dispersions, Academic Press, London, 1983.
27 R.M. Pashley, J. Colloid Interface Sci., 83 (1981) 531.
28 J.D. Sherwood, PCH, Physicochem. Hydrodyn., 10 (1988) 3.
29 R.D. Cohen, J. Membr. Sci., 32 (1987) 93.
30 V.M. Starov and D.N. Petsev, Khim. Tekhnol. Vody, 12 (1990) 791.
31 A.G. Fane, J. Membr. Sci., 20 (1984) 249.
32 A. Einstein, Ann. Phys. (Leipzig), 17 (1905) 549.